Monthly Notices of the ROYAL ASTRONOMICAL SOCIETY

MNRAS **483,** L33–L36 (2019) doi:10.1093/mnrasl/sly208
Advance Access publication 2018 November 10

On the possibility of detecting ultrashort period exoplanets with LISA

Kaze W. K. Wong [1]★ Emanuele Berti [1,2] William E. Gabella[3] and Kelly Holley-Bockelmann[3,4]

[1] *Department of Physics and Astronomy, Johns Hopkins University, Baltimore, MD 21218, USA*
[2] *Department of Physics and Astronomy, The University of Mississippi, MS 38677, USA*
[3] *Vanderbilt University, Nashville, TN37235 , USA*
[4] *Fisk University, Nashville, TN 37208, USA*

Accepted 2018 November 5. Received 2018 November 5; in original form 2018 August 31

ABSTRACT

Cunha, Silva & Lima recently reexamined the possibility of detecting gravitational waves from exoplanets, claiming that three ultrashort period systems would be observable by LISA. We revisit their analysis and conclude that the currently known exoplanetary systems are unlikely to be detectable, even assuming a LISA observation time $T_{\rm obs} = 4$ yr. Conclusive statements on the detectability of one of these systems, GP Com b, will require better knowledge of the system's properties, as well as more careful modelling of both LISA's response and theG alactic confusion noise. Still, the possibility of exoplanet detection with LISA is interesting enough to warrant further study, as gravitational waves could yield dynamical properties that are difficult to constrain with electromagnetic observations.

Key words: gravitational waves.

The idea of using space-based gravitational-wave (GW) observations with LISA to detect exoplanets was proposed almost 20 yr ago. At the time only about 20 such systems were known. Even taking into account that eccentric systems could produce significant GW power at higher harmonics, and that some of these exoplanets could resonantly excite the oscillation modes of the star they are orbiting, none of them was found to be detectable (Ferrari et al. 2000; Berti & Ferrari 2001a,b).

However, the number of known exoplanets is now in the thousands and exoplanet surveys point to a very large population of planetary systems in our Galaxy, with more than one planet per star on average (Cassan et al. 2012) and free-floating planets outnumbering the stars (Mróz et al. 2017). Many of these planetary systems are dramatically different than our own, with hot Jupiters, highly eccentric and inclined orbits, as well as entire systems of tightly packed inner planets. Such a rich and varied population of exoplanetary systems strains our current understanding of planetary system formation and evolution. A few years ago Ain, Kastha & Mitra (2015) showed that the stochastic GW background produced by these systems would peak at $\sim 10^{-5}$ Hz, with characteristic amplitude about two orders of magnitude below LISA's sensitivity, though as the exoplanet discovery space expands, our estimates of this background will evolve.

Cunha et al. (2018) recently revisited the possibility of detecting exoplanets with LISA. They computed the characteristic strain for some ultrashort period exoplanets from an online catalogue,[1] and claimed that three systems (GP Com b, V396 Hya b, and J1433 b) have characteristic GW strains large enough to be observable using the original LISA design (henceforth 'Classic LISA'; Larson, Hiscock & Hellings 2000) in one year of integration, ignoring the galactic confusion noise: cf. fig. 2 of Cunha et al. (2018).

In Table 1 we collected all relevant known properties (to the best of our knowledge) for these three systems. Note that the companions of GP Com b and V396 Hya b have masses in the exoplanet range, but they are donors of AM CVn-type interacting binaries (Kupfer et al. 2016), while J1433 b consists of an irradiated brown-dwarf companion to an accreting white dwarf (Hernández Santisteban et al. 2016). Therefore the classification of these three binaries as exoplanetary systems is, at best, debatable.

Given the GW strain amplitude $h(t)$, the characteristic strain $h_{\rm c}$ for a monochromatic circular binaries with orbital frequency $f_{\rm orb} = 2\pi/P$ emitting GWs at frequency $f = 2f_{\rm orb}$ over an observation time $T_{\rm obs}$ can be defined as $h_{\rm c} = \left[2f \int_0^{T_{\rm obs}} {\rm d}t\, h(t)^2\right]^{1/2}$ (Moore, Cole & Berry 2015). In Fig. 1 we follow the conventions established in Robson, Cornish & Liu (2018) – cf. e.g. their fig. 6 – to plot the characteristic strain along with the *effective non-sky averaged* noise power spectral density of various LISA designs for two readout channels, related to the sky-averaged noise power spectral density by $S_n(f) = \frac{3}{10} S_n^{\rm SA}(f)$ (Robson et al. 2018).[2] Brown tri-

[1] http://exoplanet.eu/catalog/

[2] We remark that this convention differs from the conventions used in Cutler (1998) and Berti, Buonanno & Will (2005), where the SNRs coming from the

★ E-mail: kazewong@jhu.edu

Table 1. Parameters of the most promising exoplanetary systems for GW detection (note that, as discussed in the text, the classification of these systems as exoplanets is questionable). All parameters are taken from the online exoplanet catalogue http://exoplanet.eu/catalog/, with the exception of quantities labelled with † (from Gaia Collaboration 2018), ‡ (from Kupfer et al. 2016), § (from Hernández Santisteban et al. 2016), and ∗(from Cunha et al. 2018). Here D_L, $M_{\rm star}(\mathrm{M}_\odot)$, and $M_{\rm planet}(\mathrm{M_J})$ denote the luminosity distance, mass of the star in solar masses, and mass of the planet in Jupiter masses, respectively, while $(\bar{\theta}_S, \bar{\phi}_S)$, ι and P denote the sky location (in ecliptic coordinates), inclination, and orbital period of the binary, respectively.

Name	D_L (pc)	$M_{\rm star}(\mathrm{M}_\odot)$	$M_{\rm planet}(\mathrm{M_J})$	$\bar{\theta}_S$ (deg)	$\bar{\phi}_S$ (deg)	ι(deg)	P (d)
GP Com b	72.83 ± 0.32†	0.435‡	26.2 ± 16.6	23.00†	187.72†	55.5 ± 22.5	0.032
V396 Hya b	93.51 ± 1.29†	0.345‡	18.3 ± 12.2	−14.50†	205.73†	52 ± 27	0.045∗
J1433 b	224.52 ± 10.22†	0.8 ± 0.07§	57.1 ± 0.7	23.89†	212.37†	84.36	0.054

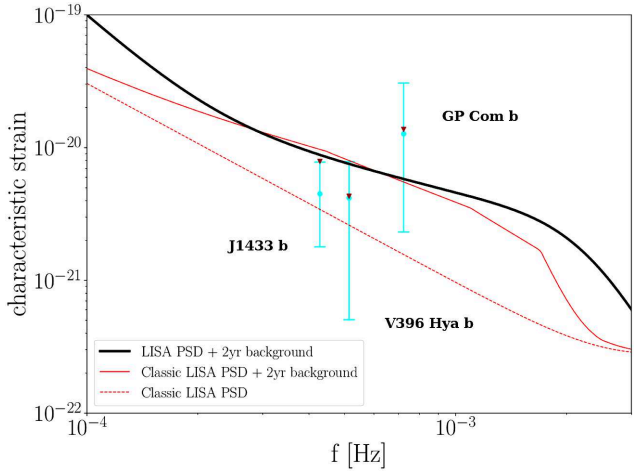

Figure 1. Characteristic strain h_c of the loudest exoplanetary candidates plotted along with $\sqrt{f\,S_n(f)}$, where $S_n(f)$ is the *effective non-sky averaged* noise power spectral density for Classic LISA without galactic confusion noise (dashed red; Larson et al. 2000), as adopted in Cunha et al. (2018); Classic LISA with galactic confusion noise (solid red); and the current LISA design with galactic confusion noise (solid black; Robson et al. 2018). The galactic confusion background and h_c are computed assuming $T_{\rm obs} = 2$ yr. Cyan dots with error bars correspond to the non-sky averaged SNR, allowing for uncertainties on the source parameters; brown inverted triangles correspond to the sky- and orientation-averaged SNR.

angles correspond to the sky-averaged characteristic strain (solid black Robson et al. 2018), while cyan error bars correspond to the range of h_c consistent with uncertainties in the source parameters (cf. Table 1). The case for detectability of these three systems with either the current or Classic LISA design based on a characteristic strain calculation is, at best, inconclusive.

As discussed in Robson et al. (2018), plots of the characteristic strain h_c are useful as rough assessments of detectability, but any conclusions must ultimately be based on a signal-to-noise ratio (SNR) calculation. For monochromatic sources, the SNR is defined as $\rho = (h|h)^{1/2}$, where

$$(h|h) = \frac{2}{S_n(f)} \int_0^{T_{\rm obs}} \mathrm{d}t\; h(t)^2. \tag{1}$$

To claim detectability, the source of interest must have SNR ρ larger than a certain threshold, which for monochromatic systems is usually taken to be $\rho_{\rm thr} = 5$ (Kupfer et al. 2018). This is somewhat optimistic: the Mock LISA Data Challenges suggest that $\rho_{\rm thr}$ is likely to be larger than 5 (Błaut, Babak & Królak 2010). Crowder & Cornish (2007) even report undetected sources with $\rho \sim 10$, though this will likely improve with more research in GW data analysis.

Unfortunately, Cunha et al. (2018) did not quantify the SNR of these systems. Furthermore, they used the outdated 'Classic LISA' noise curve (Larson et al. 2000) and they did not take into account the fact that galactic binaries produce a significant confusion noise, which is important at the frequencies of interest for exoplanetary systems. Here we revisit their analysis for the three planetary systems that are most promising for GW detection. We use updated parameters for these systems (including uncertainties, when available) and we adopt the most recent estimates for the LISA sensitivity curve, including galactic confusion noise. The parameters of the three systems under consideration are listed in Table 1.

We model the motion of the LISA detector and compute the SNR using a non-spinning, quasi-circular time-domain waveform following Cutler (1998), so that $h(t)$ is given by

$$h(t) = \frac{\sqrt{3}}{2} \frac{2\mathcal{M}^{5/3}}{D_{\rm L}} (\pi f)^{2/3} \tilde{A}(t) \times \cos\left(\int_0^t 2\pi f(t')\mathrm{d}t' + \varphi_{\rm p}(t) + \varphi_{\rm D}(t) \right), \tag{2}$$

where $f(t')$ is given in equation (1.3) of Poisson & Will (1995). Here $\tilde{A}(t)$, $\varphi_{\rm p}(t)$, and $\varphi_{\rm D}(t)$ are the amplitude modulation, polarization phase, and Doppler phase, respectively, due to LISA's motion (see Appendix for details). For a binary with component masses and total mass $M = m_1 + m_2$ the waveform depends on nine parameters: luminosity distance $D_{\rm L}$, chirp mass $\mathcal{M} = \eta^{3/5} M$, symmetric mass ratio $\eta = m_1 m_2 / M^2$, time of coalescence t_c, phase of coalescence ϕ_c, sky location $(\bar{\theta}_S, \bar{\phi}_S)$, and orbital angular momentum direction $(\bar{\theta}_L, \bar{\phi}_L)$. The overbar means that the sky location and binary orientation angles are defined in ecliptic coordinates. In order to give an estimate of the possible range of SNR, for each source we create Monte Carlo samples based on the parameter uncertainties listed in Table 1. Our waveforms depend on the sky location in the Solar system barycenter frame, while the sky location $(\theta_S^{\rm eq}, \phi_S^{\rm eq})$ and inclination ι are given in equatorial coordinates (electromagnetic observations do not give information on the polarization angle ψ). In order to translate the waveform from the Solar system barycenter frame to an Earth-centred frame, we must solve for the geometric angles in ecliptic coordinates as functions of geometric angles in equatorial coordinates. Translating the sky location from ecliptic coordinates to equatorial coordinates is trivial, but the mapping from the orbital angular momentum direction to the inclination angle is more complicated. Therefore we draw samples in the LISA (Solar system barycenter frame) coordinates, compute the SNR, and display the maximum and minimum SNRs which are consistent with the parameter uncertainties of each source. Our results, which we have checked to be in agreement with the sky location and orientation averaged results of Robson et al. (2018), are shown in Table 2.

strain amplitudes h_α ($\alpha = 1, 2$) in the two channels are added in quadrature and $S_n(f) = \frac{3}{20} S_n^{\rm SA}(f)$.

Table 2. SNR for the loudest sources considered in Cunha et al. (2018), using the noise power spectral density for Classic LISA (columns 2, 3, and 4; Larson et al. 2000) and the current LISA design (columns 5 and 6; Robson et al. 2018). The second row indicates whether we included galactic confusion noise or not. The third row lists the assumed observation time $T_{\rm obs}$ (in yr). Numbers in square brackets are the maximum and minimum SNRs consistent with parameter uncertainties for the given source. In round parentheses we report the sky location and orientation averaged SNR.

	Classic LISA			LISA	
Confusion	No	No	Yes	Yes	Yes
$T_{\rm obs}$ (yr)	1	2	2	2	4
GP Com b	$5.56^{[13.91]}_{[0.97]}$ (6.20)	$8.05^{[19.37]}_{[1.38]}$ (8.76)	$2.29^{[5.51]}_{[0.39]}$ (2.49)	$2.03^{[4.87]}_{[0.35]}$ (2.21)	$3.31^{[8.05]}_{[0.54]}$ (3.62)
V396 Hya b	$1.21^{[2.04]}_{[0.14]}$ (1.17)	$1.73^{[3.01]}_{[0.19]}$ (1.65)	$0.56^{[0.98]}_{[0.06]}$ (0.54)	$0.52^{[0.92]}_{[0.06]}$ (0.50)	$0.82^{[1.37]}_{[0.09]}$ (0.76)
J1433 b	$1.12^{[1.61]}_{[0.41]}$ (1.63)	$1.52^{[2.28]}_{[0.55]}$ (2.30)	$0.54^{[0.80]}_{[0.20]}$ (0.81)	$0.50^{[0.74]}_{[0.18]}$ (0.75)	$0.73^{[1.11]}_{[0.27]}$ (1.11)

If we fix the detectability threshold at $\rho_{\rm thr} = 5$, none of the currently known systems has $\rho > \rho_{\rm thr}$, even assuming coherent integration over the nominal LISA mission lifetime, i.e. $T_{\rm obs} = 4$ yr (Amaro-Seoane et al. 2017). GP Com b – whose companion is a donor in an AM CVn-type interacting binary (Kupfer et al. 2016), so it can hardly be classified as an exoplanet – would be marginally detectable with the 'Classic LISA' design, and it is marginally detectable by the current LISA design in four years only if we consider the most optimistic SNR values allowed by parameter uncertainties. A more reliable assessment of the detectability of this system will require better knowledge of the system's properties, as well as more careful modeling of LISA's response and of the galactic confusion noise (see e.g. Timpano, Rubbo & Cornish 2006). For V396 Hya b and J1433 b, the SNR is always lower than the detection threshold. Detection thresholds can be lowered if we incorporate information from electromagnetic measurements into the GW search, but a quantitative assessment of this issue is beyond the scope of this paper (see e.g. Shah & Nelemans 2014).

The search for ultrashort period exoplanets is certainly an exciting scientific target for LISA. We hope that our considerations will motivate further work to optimize data analysis methods, to reduce the noise power spectral density at low frequencies, and to improve our understanding of the galactic confusion noise. It will be interesting to model the exoplanet parameter space that would be detectable by LISA (including galactic exoplanets and brown dwarf populations) to better understand the potential of GW observations and their complementarity with respect to traditional detection methods.

ACKNOWLEDGEMENTS

KWKW and EB are supported by NSF Grants No. PHY-1841464 and AST-1841358, and by NASA ATP Grant 17-ATP17-0225. We thank the referee (Neil Cornish), Quentin Baghi, Robert Caldwell, Tyson Littenberg, Travis Robson, Ira Thorpe, Nadia Zakamska, Hsiang-Chih Hwang, Kevin Schlaufman, and all members of the NASA LISA Study Team for useful discussions.

REFERENCES

Ain A., Kastha S., Mitra S., 2015, Phys. Rev., 91, 124023
Amaro-Seoane P. et al., 2017, preprint (arXiv:1702.00786)
Berti E., Ferrari V., 2001a, ICTP Lect. Notes Ser., 3, 371
Berti E., Ferrari V., 2001b, Phys. Rev., 63, 064031
Berti E., Buonanno A., Will C. M., 2005, Phys. Rev., 71, 84025
Błaut A., Babak S., Królak A., 2010, Phys. Rev., 81, 63008
Cassan A. et al., 2012, Nature, 481, 167
Crowder J., Cornish N. J., 2007, Class. Quantum Gravity, 24, S575
Cunha J. V., Silva F. E., Lima J. A. S., 2018, MNRAS, 480, L28
Cutler C., 1998, Phys. Rev., 57, 7089
Ferrari V., Berti E., D'Andrea M., Ashtekar A., 2000, Int. J. Mod. Phys., 9, 495
Gaia Collaboration et al., 2018, A&A, 616, A1
Hernández Santisteban J. V. et al., 2016, Nature, 533, 366
Kupfer T., Steeghs D., Groot P. J., Marsh T. R., Nelemans G., Roelofs G. H. A., 2016, MNRAS, 457, 1828
Kupfer T. et al., 2018, MNRAS, 480, 302
Larson S. L., Hiscock W. A., Hellings R. W., 2000, Phys. Rev., 62, 62001
Moore C. J., Cole R. H., Berry C. P. L., 2015, Class. Quantum Gravity, 32, 15014
Mróz P. et al., 2017, Nature, 548, 183
Poisson E., Will C. M., 1995, Phys. Rev., 52, 848
Robson T., Cornish N., Liu C., 2018, preprint (arXiv:1803.01944)
Shah S., Nelemans G., 2014, ApJ, 790, 161
Timpano S. E., Rubbo L. J., Cornish N. J., 2006, Phys. Rev., 73, 122001

APPENDIX: ANTENNA PATTERN

In this Appendix we write down, for completeness, the antenna pattern expressions used in our non-angle-averaged SNR calculation. Following Cutler (1998), we denote the LISA-based coordinate system by unbarred quantities, while barred quantities refer to the fixed ecliptic coordinate system. The amplitude modulation in equation 2 is given by

$$\tilde{A}(t) = \sqrt{\left[1 + (\hat{\boldsymbol{L}} \cdot \boldsymbol{n})^2\right]^2 F_+{}^2 + 4(\hat{\boldsymbol{L}} \cdot \boldsymbol{n})^2 F_\times{}^2}, \tag{A1}$$

where $\hat{\mathbf{L}}$ and $-\mathbf{n}$ are the unit vector along the binary's orbital angular momentum and the GW direction of propagation, respectively. The pattern functions F_+ and $F_\times$ are defined as

$$\begin{aligned} F_+(\theta_S, \phi_S, \psi_S) &= \tfrac{1}{2}(1 + \cos^2\theta_S)\cos 2\phi_S \cos 2\psi_S \\ &\quad - \cos\theta_S \sin 2\phi_S \sin 2\psi_S, \\ F_\times(\theta_S, \phi_S, \psi_S) &= \tfrac{1}{2}(1 + \cos^2\theta_S)\cos 2\phi_S \sin 2\psi_S \\ &\quad + \cos\theta_S \sin 2\phi_S \cos 2\psi_S. \end{aligned} \tag{A2}$$

The angles (θ_S, ϕ_S) specify the source location, while ψ_S denotes the the polarization angle:

$$\tan\psi_S(t) = \frac{\hat{\boldsymbol{L}} \cdot \boldsymbol{z} - (\hat{\boldsymbol{L}} \cdot \boldsymbol{n})(\boldsymbol{z} \cdot \boldsymbol{n})}{\boldsymbol{n} \cdot (\hat{\boldsymbol{L}} \times \boldsymbol{z})}, \tag{A3}$$

where $\mathbf{z}$ is the unit normal to the LISA detector plane.

The scalar products can be written as

$$\boldsymbol{z} \cdot \boldsymbol{n} = \cos\theta_S, \tag{A4}$$

$$\hat{\boldsymbol{L}} \cdot \boldsymbol{z} = \tfrac{1}{2}\cos\bar{\theta}_L - \tfrac{\sqrt{3}}{2}\sin\bar{\theta}_L \cos(\bar{\phi}(t) - \bar{\phi}_L), \tag{A5}$$

$$\hat{\boldsymbol{L}} \cdot \boldsymbol{n} = \cos\bar{\theta}_L \cos\bar{\theta}_S + \sin\bar{\theta}_L \sin\bar{\theta}_S \cos(\bar{\phi}_L - \bar{\phi}_S), \tag{A6}$$

and

$$\boldsymbol{n}\cdot(\hat{\boldsymbol{L}}\times\boldsymbol{z}) = \frac{1}{2}\sin\bar{\theta}_L\sin\bar{\theta}_S\sin(\bar{\phi}_L-\bar{\phi}_S) - \frac{\sqrt{3}}{2}\cos\bar{\phi}(t)\left(\cos\bar{\theta}_L\sin\bar{\theta}_S\sin\bar{\phi}_S - \cos\bar{\theta}_S\sin\bar{\theta}_L\sin\bar{\phi}_L\right) - \frac{\sqrt{3}}{2}\sin\bar{\phi}(t)\left(\cos\bar{\theta}_S\sin\bar{\theta}_L\cos\bar{\phi}_L - \cos\bar{\theta}_L\sin\bar{\theta}_S\cos\bar{\phi}_S\right). \quad \text{(A7)}$$

The polarization and Doppler phases in equation (2) are given by

$$\varphi_{\rm p}(t) = \tan^{-1}\left[\frac{2(\hat{\boldsymbol{L}}\cdot\boldsymbol{n})F_\times(t)}{(1+(\hat{\boldsymbol{L}}\cdot\boldsymbol{n})^2)F_+(t)}\right] \quad \text{(A8)}$$

$$\varphi_{\rm D}(t) = \tfrac{2\pi f}{c}R\sin\bar{\theta}_S\cos(\bar{\phi}(t)-\bar{\phi}_S), \quad \text{(A9)}$$

where R = 1AU and $\bar{\phi}(t) = \bar{\phi}_0 + 2\pi t/T$. Here $T = 1$ yr is the orbital period of LISA, and $\bar{\phi}_0$ is a constant specifying the detector's location at time $t = 0$.

Assuming no precession of the orbital angular momentum, the time-dependent LISA related angles (θ_S, ϕ_S, ψ_S) can be expressed in terms of the time-independent angles defined in the ecliptic coordinates ($\bar{\theta}_S$, $\bar{\phi}_S$, $\bar{\theta}_L$, $\bar{\phi}_L$) through the following relations:

$$\cos\theta_S(t) = \tfrac{1}{2}\cos\bar{\theta}_S - \tfrac{\sqrt{3}}{2}\sin\bar{\theta}_S\cos(\bar{\phi}(t)-\bar{\phi}_S), \quad \text{(10a)}$$

$$\phi_S(t) = \alpha_0 + \frac{2\pi t}{T} + \tan^{-1}\left[\frac{\sqrt{3}\cos\bar{\theta}_S + \sin\bar{\theta}_S\cos(\bar{\phi}(t)-\bar{\phi}_S)}{2\sin\bar{\theta}_S\sin(\bar{\phi}(t)-\bar{\phi}_S)}\right], \quad \text{(10b)}$$

where α_0 is a constant specifying the orientation of the detector arms at $t = 0$.

We set $\alpha_0 = 0$ and $\bar{\phi}_0 = 0$ in our calculations, but we checked that varying α_0 and $\bar{\phi}_0$ has an insignificant effect on the SNR as long as the observation period $T_{\rm obs} \gtrsim 1$ yr.

This paper has been typeset from a TEX/LATEX file prepared by the author.